**REGULAR PAPER**

# Inverted InAlAs/InGaAs Avalanche Photodiode with Low–High–Low Electric Field Profile

Masahiro Nada*, Yoshifumi Muramoto, Haruki Yokoyama, Naoteru Shigekawa, Tadao Ishibashi, and Satoshi Kodama

*NTT Photonics Laboratories, NTT Corporation, Atsugi, Kanagawa 243-0198, Japan*

We propose a new p-down inverted avalanche photodiode (APD) structure suitable for a scaled APD with smaller junctions. The inverted APD structure has an edge-field buffer layer to prevent undesirable edge breakdown and suppress the excess surface leakage current associated with the InGaAs mesa surface. The fabricated back-illuminated InAlAs/InGaAs APDs show excellent multiplication characteristics without edge breakdown. An $f_{3dB}$ of 27 GHz and a GB product of 220 GHz are obtained for these APDs. © 2012 The Japan Society of Applied Physics

## 1. Introduction

The use of avalanche photodiodes (APDs) for achieving better photoreceiver sensitivity is still important in optical fiber communications systems with bit rates beyond 10 Gbps. Here, for sufficient responsivity, bandwidth, and multiplication gain, all the structural parameters have to be compromised. A key design for the APD structure is related to the trade-off between responsivity and bandwidth, where a higher bandwidth generally requires a thinner absorption layer, resulting in a lower responsivity. A thinner absorption layer also increases junction capacitance. For these reasons, an evanescent-coupled waveguide, in which a thinner absorption layer is allowed, has been incorporated into high-speed APDs.[1–6] However, the vertically illuminated type is favorable for minimizing polarization-dependent loss and offers easier optical coupling between the fiber and the APD active area.

For a scaled APD with smaller junctions, the fabrication process is another issue. For example, selective Zn diffusion or ion implantation techniques (although common to 10 Gbps APDs[7–10]) are not necessarily applicable to further scaling.

In this paper, we propose a new p-down inverted APD structure that can be simply fabricated with double mesas and is suitable for scaling. A 3-dB bandwidth of 27 GHz and a gain-bandwidth product of 220 GHz are obtained for the fabricated InAlAs/InGaAs APDs, demonstrating the potential of the proposed structure.

## 2. Design Concept and Inverted APD Structure

Figure 1 shows a schematic cross section of the proposed inverted APD, which is suitable for high-speed operation with an electron injection scheme. The primary reason we chose the inverted (p-down) configuration is that the hybrid-absorption layer (p- and depleted InGaAs), which we call the maximized-induced current (MIC) design,[11] can easily be incorporated into mesa-type devices. Unlike in the case of APDs for 10 Gbps operation, a high-speed APD (e.g., $f_{3dB} > 20$ GHz) with a conventional geometry strictly loses responsivity as its bandwidth must be increased. This type of tradeoff can be better relaxed by incorporating the MIC design. Namely, given the total absorption layer thickness, the carrier transit time can be minimized by adjusting the ratio between the two absorption layers, and the $f_{3dB}$ determined by such a means is much larger than that for a depleted absorber or a uni-travelling carrier absorber.[12]

Simultaneously, the optimum set of hybrid absorbers gives the maximum responsivity for a required $f_{3dB}$.

Why is the "inverted" configuration needed? In the proposed structure, the top mesa is formed with a widegap n-contact layer, leaving the edge-field buffer layer on the avalanche layer. The second mesa consists of layers from the absorption to edge-field buffer layer with a "terrace" of several micrometers surrounding the top mesa. By this layer configuration, the top n-contact mesa can define the APD active layer and allow the use of a p-type absorber placed beneath it. On the other hand, the reported structure with a widegap p-type top mesa[13] cannot define the APD active area as long as the p-type absorber is arranged beneath it.

When the device is biased, the edge-field (field concentration) is inherently induced in the bottom periphery region of the n-type top mesa. To avoid this effect on the breakdown behavior, the parameters of the edge-field buffer, and p- and n-type field control layers have to be carefully designed.

The calculated field profile in the central active region of an InAlAs/InGaAs inverted APD at an operation voltage (assuming a multiplication factor $M = 10$) is shown in Fig. 2. The field profile typically has a "low–high–low" shape. The electric field in the undoped absorption and edge-field buffer layers can be controlled by adjusting the sheet doping concentrations of the p- and n-type field control layers. The edge-field effect, as described above, increases the field intensity locally in the edge-field buffer layer. However, the field in the edge-field buffer layer is designed to be sufficiently low. When the thickness of the edge-field buffer layer is made moderately wide, the edge field in the avalanche layer is relaxed inversely. The variation in the electric field profile of InAlAs/InGaAs APD with reverse bias voltage is shown in Fig. 3. In a voltage range from 0 to 10 V, only the p- and n-field control layers are depleted, and beyond that voltage range the depletion starts to spread to the edge-field buffer layer. At 14 V, a field in the undoped InGaAs absorption layer is induced, which is the onset voltage ($V_{on}$) of photocurrent flow. In the terrace area, on the other hand, further depletion is terminated at a voltage when the depletion of the edge-field buffer layer is completed. This situation realizes the low-field condition for the InGaAs absorption layer at the mesa edge. Because the device active area is defined by the n-type mesa, the junction capacitance contributed by the terrace region is negligible. Furthermore, low fields in the undoped-absorption layer and the sidewall of the second mesa at the operation voltage achieve a low surface leakage

*E-mail address: nada.masahiro@lab.ntt.co.jp
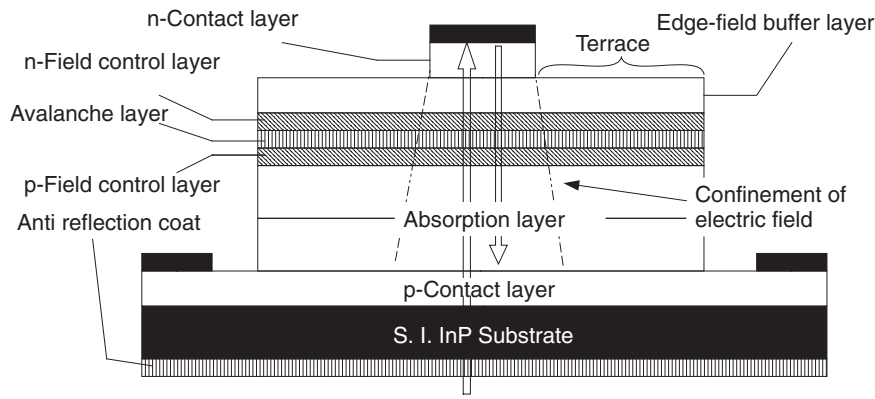
**Fig. 1.** Schematic cross section of proposed p-down inverted APD structure.
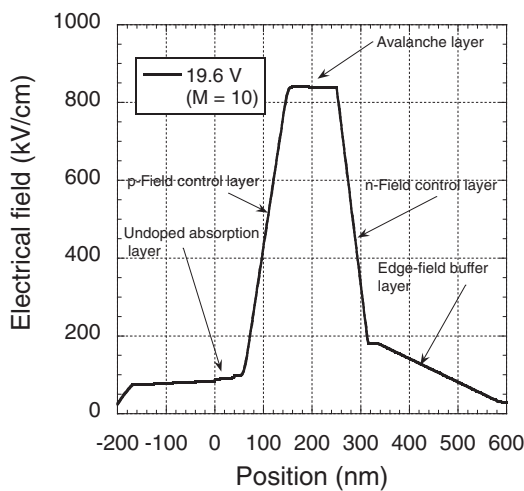


**Fig. 2.** Calculated electric field profile of inverted InAlAs/InGaAs APD at operation voltage of 19.6 V ($M = 10$).
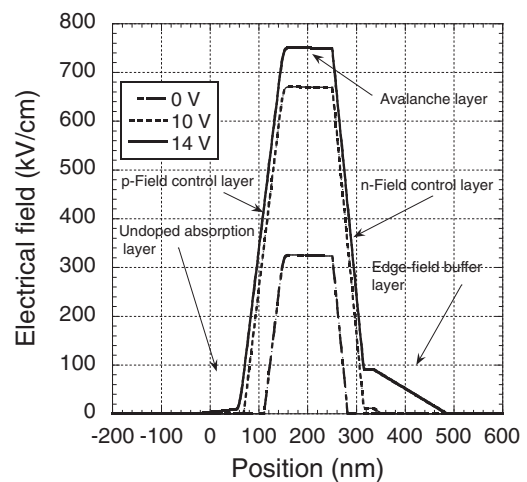


**Fig. 3.** Calculated electric field profile of InAlAs/InGaAs APD when increasing bias voltage.

current. These can provide suitability for scaling and device stability.

## 3. Experimental Procedure

### 3.1 Sample fabrication

The epitaxial layers consist of p-contact, graded doped p-type absorption, undoped absorption, p-type field control (90 nm), InAlAs avalanche, n-type field control (65 nm), n-type InP edge-field buffer (250 nm), and n-contact layers. All the layers were grown on semi-insulating InP substrate by metal–organic vapor phase epitaxy (MOVPE). The total thickness of the absorption layer was 400 nm. The avalanche layer thickness of 100 nm was chosen to maximize the gain-bandwidth product, although such a value is close to the lower limit where tunneling current becomes dominant in the dark current. In this case, the p- and n-field control layers have doping concentrations of $6 \times 10^{17}$ and $7 \times 10^{17}$ cm$^{-3}$, respectively, to make a "low–high–low" electric field profile around the avalanche layer.

The back-illuminated mesa-type APDs were fabricated by a conventional technique using chemical wet-etching and metal lift-off processes. For electrode interconnection, the mesa was embedded in a benzocyclobutene (BCB) layer covered with SiN deposited by plasma-enhanced chemical

vapor deposition. A metal mirror was also formed on the n-contact layer with a SiN inter layer. The diameter of the top mesa (n-contact layer) that defines the device active area ranges from 10 to 20 µm.

### 3.2 APD characterization

In addition to $I$–$V$ measurements (under dark and illumination conditions), $C$–$V$ measurements were performed to study how junction depletion proceeds with applied voltage. To confirm its origin, the dependence of dark current on temperature was also determined. The frequency photoresponse of a fabricated APD was on-wafer-characterized using an optical component analyzer.

## 4. Results and Discussion

Figure 4 shows the $I$–$V$ characteristics under dark and illumination conditions for a fabricated APD with a top mesa diameter of 10 µm. The voltages at which the photocurrent starts to flow normally ($V_{on}$) and the breakdown voltage ($V_{br}$) were 13.1 and 22.8 V, respectively. The photocurrent and dark current near the $V_{br}$ behave as expected for avalanche breakdown. These results imply that no undesirable breakdown, such as edge breakdown, occurs. The incident optical power was 7.4 µW in the measurement, so, the product of
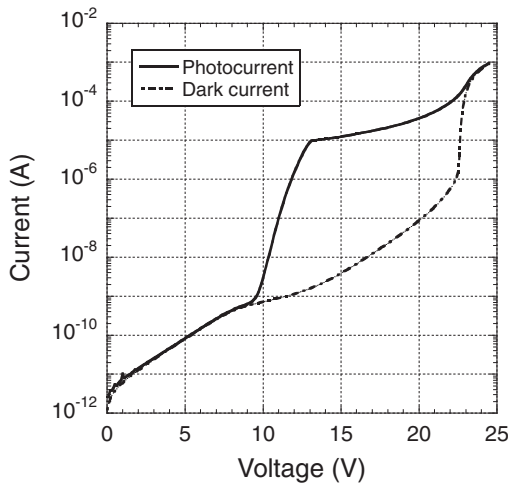
**Fig. 4.** Measured *I–V* characteristics of fabricated APD with diameter of 10 μm.
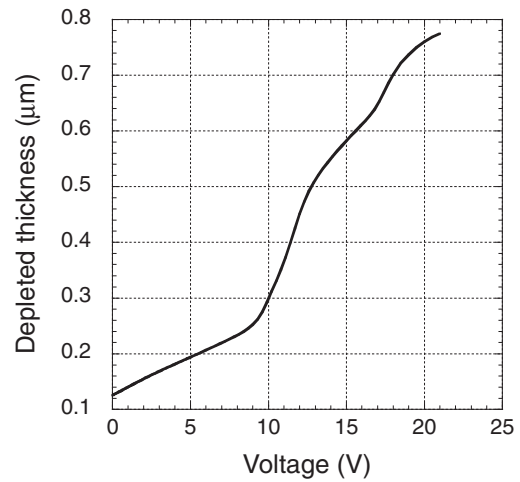


**Fig. 6.** Depletion thickness for voltage evaluated from measured *C–V* characteristics for inverted InAlAs/InGaAs APD structure.
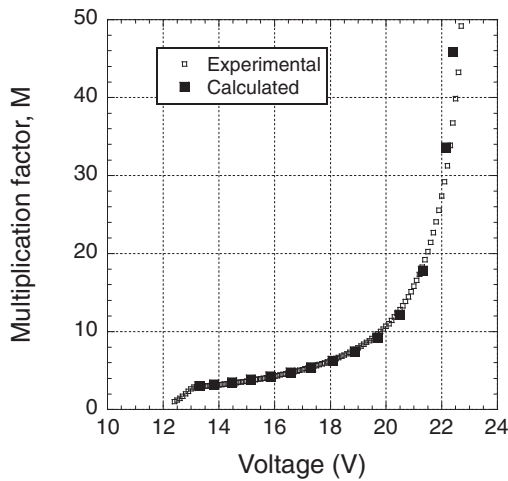


**Fig. 5.** Voltage dependences of experimental and calculated multiplication factors.
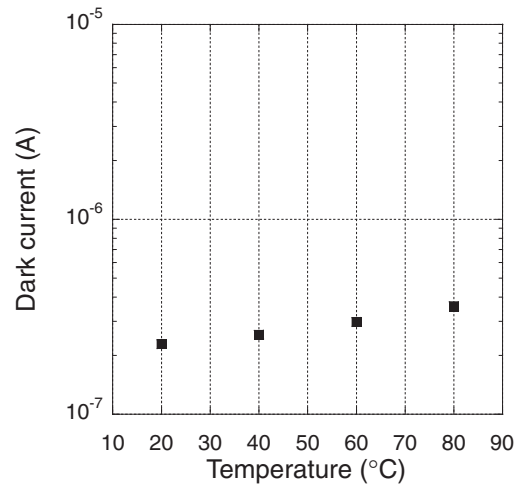


**Fig. 7.** Temperature dependence of dark current of fabricated APD at 0.9 $V_{br}$. The diameter of the device is 20 μm.

responsivity ($R$) and multiplication factor ($M$), $MR$, is 1.35 A/W at $V_{on} = 13.1$ V. Although the responsivity $R$ is not obtained independently, by fitting the experimental *I–V* data with the calculated $M$, both $R$ and $M$ can be estimated.

Figure 5 shows the result of the curve fitting of the measured $M$ (□) with the calculated $M$ (■) using reported ionization rates in InAlAs,[14] where the doping levels for the p- and n-field control layers were slightly adjusted so that the calculated $V_{on}$ and $V_{br}$ coincide with those of the experiments. Consequently, $M$ and $R$ are respectively determined to be 3.2 and 0.42 A/W at $V_{on} = 13.1$ V. $R = 0.42$ A/W is slightly smaller than its calculated value of 0.49 A/W assuming an InGaAs absorber thickness of 400 nm, a top metal reflection of 95%, and 100% optical coupling.

Depletion thickness as a function of applied bias voltage, evaluated from the *C–V* data, is shown in Fig. 6. It increases slowly at voltages up to 9 V followed by a rapid increase in the voltage range from 9 to 13 V. Then, more gradual depletion finally extends to 0.8 μm. From the designed layer thicknesses and the $V_{on}$ of 13 V obtained from *I–V*

measurement, the first voltage region (<9 V) is found to be where the n-field control layer is being depleted. Then, the depletion spreads to the edge-field buffer layer for $V > 9$ V. At approximately 14 V, a weak inflection point appears, corresponding to the depletion of the p-field control layer, and further depletion reaches a width of 0.8 μm. These variations in depletion width with voltage fairly agree with the calculated results in Fig. 3.

A multiplication factor of 10 was achieved at 19.6 V (0.86 $V_{br}$) with a multiplied dark current of 65 nA, which is sufficiently low not to affect the noise current during APD operation.

Figure 7 shows the temperature dependence of the dark current at a bias of 0.9 $V_{br}$ giving an $M$ of 15. The diameter of the top mesa of the device is 20 μm. With increasing temperature from 20 to 80 °C, dark current very slowly rises from 230 to 350 nA, which shows an increase of 56%. This value is consistent with the calculated ones estimated from the temperature dependence of the band gap of InAlAs.[15] This indicates that the major component of the dark current
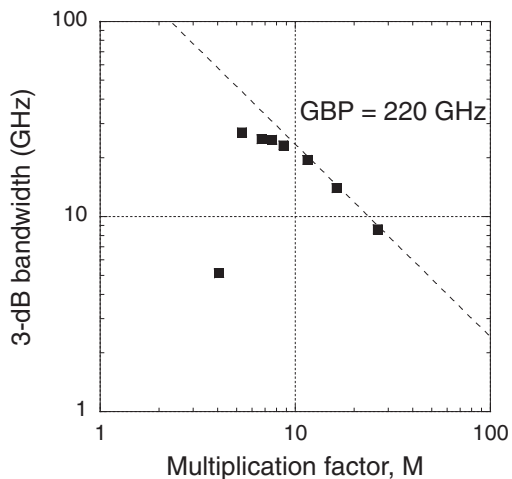
**Fig. 8.** $f_{3dB}$ of APD depending on $M$.

of this inverted APD is not surface leakage current associated with the InGaAs mesa but tunneling current in the InAlAs avalanche layer. It seems that the field is confined effectively to the central region of the APD, and that the field at the InGaAs mesa sidewall is sufficiently low, which is important for realizing reliable APDs.

Figure 8 shows the gain-bandwidth characteristics of a fabricated InAlAs/InGaAs APD. The diameter of the device is $10\,\mu m$. From the characteristics, the gain-bandwidth product (GB) of the APD is evaluated to be $220\,GHz$, which is comparable to the best value reported for an InAlAs/InGaAs APD.[16] A maximum $f_{3dB}$ of $27\,GHz$ is obtained at $M = 5.3$ and an $f_{3dB} > 24\,GHz$ is maintained at $M < 8$. To the best of our knowledge, these $f_{3dB}$ values are the largest ever reported for a vertically illuminated APD.

The DC photocurrent starts to flow at $V_{on}$ of $13\,V$ with $M = 3.2$, while the RF response emerges at a higher bias, i.e., at $V > 17\,V$ with $M > 5.3$ in this APD. This voltage interval ($\Delta V = 4\,V$) is relatively small and close to the minimum necessary to induce a certain field ($> 50\,kV/cm$) to reach a high saturation velocity of holes in the InGaAs layer.

## 5. Conclusions

We have proposed and demonstrated a new p-down inverted APD structure suitable for a scaled APD with smaller junctions required for high-speed operation. This APD structure includes a double-mesa geometry, an MIC-absorption layer design, and an edge-field buffer layer. The combination of the low–high–low field profile obtained using the additional edge-field buffer layer and the inverted layer arrangement is essential to prevent undesirable edge breakdown and excess surface leakage current associated with the InGaAs mesa surface. Back-illuminated InAlAs/InGaAs APDs are fabricated and characterized. An $f_{3dB}$ of $27\,GHz$ and a GB product of $220\,GHz$ are obtained for these APDs. To the best of our knowledge, these values are the largest ever reported for vertically illuminated APDs. Furthermore, we confirm that the dark current is sufficiently low and its temperature dependence is negligible.

1) J. Wei, F. Xia, and S. R. Forrest: IEEE Photonics Technol. Lett. **14** (2002) 1590.
2) C. Cohen-Jonathan, L. Giraudet, A. Bonzo, and J. P. Praseuth: Electron. Lett. **33** (1997) 1492.
3) N. Yasuoka, H. Kuwatsuka, A. Kuramata, T. Uchida, Y. Yoneda, and S. Nakai: Proc. Optical Fiber Communication Conf. (OFC), 2004, paper TuM2.
4) T. Torikai, T. Nakata, T. Kato, and K. Makita: Proc. Optical Fiber Communication Conf. (OFC), 2005, paper OFM3.
5) T. Nakata, T. Takeuchi, K. Makita, Y. Amamiya, T. Kato, Y. Suzuki, and T. Torikai: Proc. European Conf. Exhib. Optical Communication (ECOC), 2002, paper 10.5.1.
6) S. Shimizu, K. Shiba, T. Nakata, K. Kasahara, and K. Makita: Electron. Lett. **43** (2007) 476.
7) J. Wei, J. C. Dries, H. Wang, M. L. Lange, G. H. Olsen, and S. R. Forrest: IEEE Photonics Technol. Lett. **14** (2002) 977.
8) E. Yagyu, E. Ishimura, M. Nakaji, T. Aoyagi, and Y. Tokuda: IEEE Photonics Technol. Lett. **18** (2006) 1264.
9) Y. Hirota, Y. Muramoto, T. Takeshita, T. Ito, H. Ito, S. Ando, and T. Ishibashi: Electron. Lett. **40** (2004) 1378.
10) Y. L. Goh, D. J. Massey, A. R. J. Marshall, J. S. Ng, C. H. Tan, W. K. Ng, G. J. Rees, M. Hopkinson, J. P. R. David, and S. K. Jones: IEEE Trans. Electron Devices **54** (2007) 11.
11) Y. Muramoto and T. Ishibashi: Electron. Lett. **39** (2003) 1749.
12) T. Ishibashi, N. Shimizu, S. Kodama, H. Ito, T. Nagatsuma, and T. Furuta: OSA TOPS Ultrafast Electron. Optoelectron. **13** (1997) 83.
13) B. F. Levine, R. N. Sacks, J. Ko, M. Jazwiecki, J. A. Valdmanis, D. Gunther, and J. H. Meier: IEEE Photonics Technol. Lett. **18** (2006) 1898.
14) Y. L. Goh, D. J. Massey, A. R. J. Marshall, J. S. Ng, C. H. Tan, W. K. Ng, G. J. Rees, M. Hopkinson, J. P. R. David, and S. K. Jones: IEEE Trans. Electron Devices **54** (2007) 11.
15) D. K. Gaskill, N. Bottka, L. Aina, and M. Mattingly: Appl. Phys. Lett. **56** (1990) 1269.
16) M. Lahrichi, G. Glastre, E. Derouin, D. Carpentier, N. Lagay, J. Decobert, and M. Achouche: IEEE Photonics Technol. Lett. **22** (2010) 1373.